Particle Accelerators, 1971, Vol. 2, pp. 17–29

THE INTERDIGITAL H-TYPE (IH) STRUCTURE, AN ACCELERATING STRUCTURE FOR LOW ENERGY BEAMS

M. BRES, A. CHABERT, F. FORET, D. T. TRAN† and G. VOISIN
Institut de Physique Nucléaire, Université de Lyon 69-Villeurbanne, France

After a brief description of the structure, its main characteristics are deduced from the results of a series of experiments and discussed from a theoretical point of view. Its practical use in an accelerator is considered and illustrated by the outlines of the Lyon heavy-ion linear accelerator project.

1. INTRODUCTION

The first descriptions of the IH accelerating structure appeared in the literature in 1956[1] and, for a slightly different version, in 1957.[2] Since that time, a lot of interesting work on this matter has been carried on in Kharkov[3,4] and Saclay.[5] For our part, we began to study the IH structure in 1966, in a rather systematic way, both as self-supporting research program and as a basis for our heavy ion accelerator project.

From the geometrical point of view, the IH line can be compared to the Alvarez structure, except for the alternate disposition of the stems (Fig. 1), but the rf properties of its first passband are close to these of 'H-type' and Sloan and Lawrence structures.

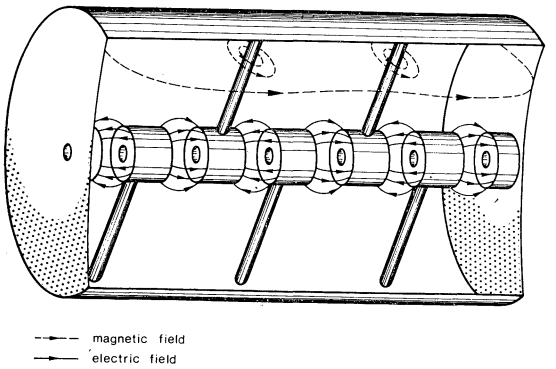

FIG. 1. General view of an IH cavity with a rough indication of the field distribution for the lowest mode.

The main characteristics of accelerating IH structures consist of their small transverse dimensions for a given frequency (typical tank diameters between 10 and 20 per cent of wavelength) and of their high efficiency in the low energy range.

For both reasons, the IH structure seems well suited for the acceleration of low energy beams, and especially in heavy ion linear accelerators.

2. MAIN CHARACTERISTICS

2.1. *Description of the accelerating mode*

The acceleration of particles involves the lowest passband of the structure. This 'stem-resonant' passband is characterized by its unusual width (between 60 and 130 per cent) and its negative group velocity.

Figure 1 gives a rough idea of the field distribution for the $5\pi/6$ mode in a 6-gap periodic cavity. Far from both drift tubes and stems, the magnetic field is almost parallel to the cavity walls (as in H-type structures), but the main part of this field whirls around the stems where most of the magnetic energy is located.

Perturbation measurements over a stem show that the magnetic field prevails near the cavity wall with no significant change along at least one half of the stem, then decreases more and more quickly in the neighbourhood of the drift tube where the electric field becomes predominant. The electric field itself is well concentrated in the gaps, accounting for the good efficiency of such accelerating structures.

As a consequence of this particular field distribution, the electric field appears to be created in the gaps by the intense currents flowing along the stems.

Due to the actual magnetic field pattern, the boundary condition cannot be satisfied on the ends of a cavity in the π mode. Consequently, the lowest mode that appears in an enclosed periodic cavity including N accelerating cells is the $\pi - \pi/N$

† Detached from Thomson-C.S.F., Domaine de Corbeville, 91-Orsay.

mode ($5\pi/6$, in the case of Fig. 1). In the same way, we intend to tune an accelerating cavity at the lowest possible mode. Then, the accelerating field cannot be kept constant from gap to gap and must vanish at both ends of the cavity. With these restrictions, the field law must be more or less sinusoidal, and the corresponding phase shift per period (measured in travelling waves) is in the neighbourhood of π, but not exactly π, and may vary from cell to cell.

In standing wave operation, however, the electric fields in two successive gaps are in opposite directions at a given instant, and the synchronism of accelerated particles can be expressed by the same law as in, strictly speaking, the π mode:

$$L = \frac{\beta\lambda}{2} \tag{1}$$

where L is the period length, λ the wave length, and β, the relative velocity of the particles.

Let us now examine in more detail the results of an experimental investigation on dispersion characteristics and efficiency of this structure.

2.2. *Dispersion characteristics*

As we said in the preceding section, the successive cells of an accelerating cavity are not tuned at cut-off mode then, for a given frequency, the transverse geometry of a cavity depends upon its length.

In order to design such a cavity (Section 4.4), it is necessary to study the dispersion curves of periodic structures as a function of their geometrical parameters.

After a series of experiments, we came to the following conclusions:

—As previously announced, the passband is always wide, and the group velocity strictly negative.

—The shape of the dispersion curve is deeply affected by the period length, as shown on Fig. 2 which presents a series of curves plotted for different period lengths, with fixed cavity, stems and drift-tubes diameters and a constant gap to period ratio of 50 per cent. Obviously, all the curves intersect at almost a same point where the resonance is not affected by large changes in the period. Moreover, the passband strongly increases when the period decreases and the group velocity remains consistent with a good mode separation in the neighbourhood of the π mode.

—As shown on Fig. 3, the influence of the other parameters affects much more the position of the curve than its shape. We shall use the effect of drift tubes and cavity diameters for tuning the successive accelerating cells, while the influence of stem diameters could be taken into account for slight adjustments of both fields and frequency.

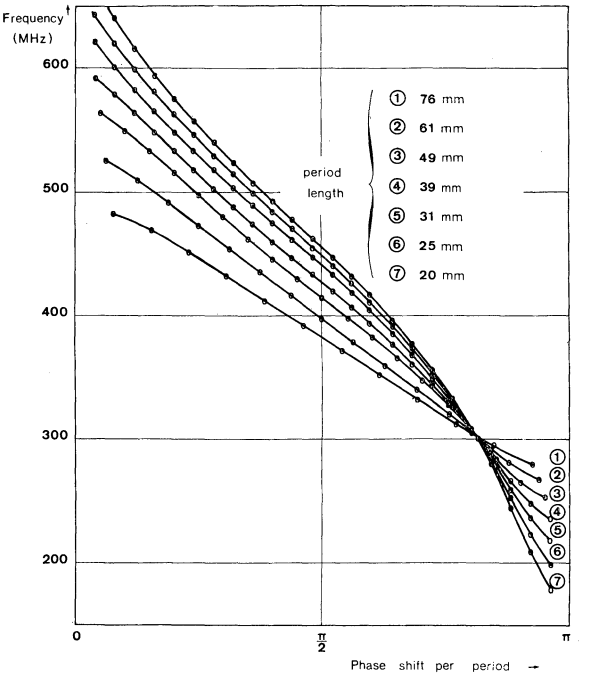

FIG. 2. Typical dispersion curves showing the effect of period length. Cavity diameter: 264 mm, drift tube diameter: 25 mm, stem diameter: 6 mm, gap to period ratio: $\frac{1}{2}$.

2.3. *Shunt impedance and quality factor*

In the next sections, we shall refer to the total effective shunt impedance of a cavity:

$$Z_s = \left(\int_0^H E\,dz\right)^2 \Big/ P, \tag{2}$$

to its effective shunt impedance per unit length:

$$z_s = Z_s/H, \tag{3}$$

and to its unloaded quality factor:

$$Q = \omega W/P, \tag{4}$$

where P represents the power losses in the whole cavity of length H, at the angular frequency of resonance ω, E, the effective accelerating field (including the time dependence, but not the synchronous phase), and W, the overall energy stored.

Unless when otherwise mentioned, our experiments were made on periodic structures, and their results must be understood for a precise energy.

As it is well known, the determination of Z_s/Q only requires perturbation measurements of the field. We used such a technique, with direct punching of both bead position along the axis and frequency on paper tape for further use in a computer. The unloaded Q was measured by a less

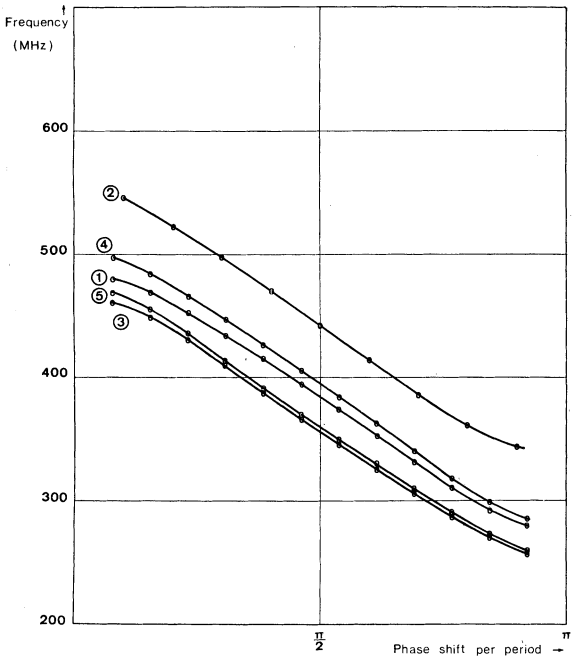

FIG. 3. Effect of different parameters on the dispersion curve. (1) cavity ϕ: 264 mm, drift tubes ϕ: 25 mm, stems ϕ: 6 mm, period length 76 mm, gap to period ratio: $\frac{1}{2}$; (2) Same as (1), except for the cavity ϕ: 211 mm; (3) Same as (1), except for the drift tubes ϕ: 31 mm; (4) Same as (1), except for the stems ϕ: 7.5 mm; (5) Same as (1), except for the gap to period ratio: $\frac{3}{8}$.

sophisticated, graphical method, by means of Smith's admittance chart.

Our first experimental result concerns the transit time factor which remains between 0.84 and 0.89—that is to say, close to the theoretical value of 0.90—over a wide range of energies, for a gap to period ratio of 50 per cent and reasonable bore diameters of the drift tubes.

Since the IH structure is not operated at cut-off frequency, the phase shift per unit length depends upon the cavity length, and it is interesting to examine the variation of Q and shunt impedance with this parameter.

A rough estimation of this dependence for Z_s/Q can be established assuming a gap voltage law in the form:

$$V_n = V\sin(n-\tfrac{1}{2})\frac{\pi}{N}, \tag{5}$$

where n is the actual index of the gap, and N, the total number of periods of the cavity. The main electric energy being concentrated in the gaps, the total energy is proportional to $\omega\Sigma V_n^2$, and Z_s/Q, to $(\Sigma V_n)^2/(\omega\Sigma V_n^2)$ leading to the law:

$$Z_s/Q \propto \lambda\left(\pi - \frac{\pi}{N}\right)\Big/\left(N\sin^2\frac{\pi}{2N}\right), \tag{6}$$

where $\lambda(\pi-\pi/N)$ is the wave length at the $\pi-\pi/N$ mode, and which obviously becomes a linear dependence as N increases.

As shown on Fig. 4, the experimental results are in good agreement with this formula.

Unfortunately, since we do not know sufficiently well the magnetic field distribution, all we can predict about the variation of Q is that it must tend to a constant value as N increases (when the losses in the end walls become negligible as compared to the cavity losses). Taking into account the inherent difficulties of Q measurements, this conclusion was fairly well verified by our experiments.

Figure 4 shows the strong increase of both Q and Z_s/Q when the diameters of the drift tubes decrease (as compared to cavity diameter). On the other hand, Fig. 5 illustrates the significant improvement of Z_s/Q and the slight increase of Q when the energy decreases (for a constant ratio of drift tubes to cavity diameters).

For both Figs. 4 and 5, as the wavelength is very sensitive to the number of periods (Fig. 2), we present in solid lines the part of each curve corresponding to the given energy within 2 per cent. As the dispersion of our Q measurements was not better than 5 per cent in the general case, we took for each cavity length the mean result of three successive experiments and the dispersion indicated on these figures corresponds to the variation of this mean value along the solid part of each curve.

The comparison of Z_s/Q and Q values shows that, especially at low energies, the IH structure presents a high efficiency due to a good concentration of the fields in spite of a moderate quality factor.

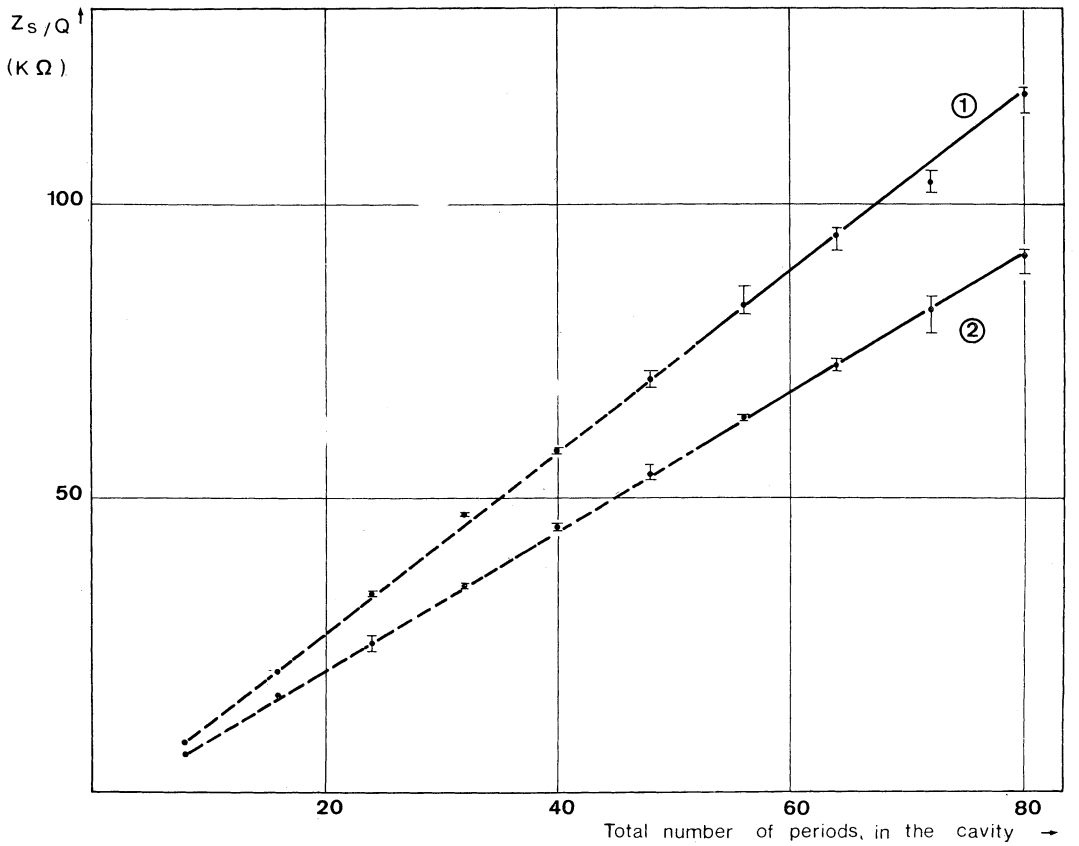

FIG. 4. Z_s/Q dependence on cavity length for different diameters of the drift tubes. (1) drift tubes ϕ: 6.66 per cent of cavity diameter; along the solid part of the curve: energy 290 keV per nucleon ± 1 per cent, average Q at 27 MHz: $15\,800 \pm 3$ per cent. (2) drift tubes ϕ: 10 per cent of cavity diameter; along the solid part of the curve: energy 190 keV per nucleon ± 1 per cent, average Q at 27 MHz: $12\,900 \pm 3$ per cent. Both curves are deduced from experimental measurements (within the indicated limits) by formula (6). Gap to period ratio: $\frac{1}{2}$.

The results of our experiments in terms of shunt impedance per unit length will be described in Section 4.2, where the question of optimum energy range of the structure will be discussed.

3. THEORETICAL ASPECTS

Due to the actual distribution of the fields, which obviously presents no symmetry of revolution, the exact calculation of an IH structure leads to a complicated three-dimensional problem.

For this purpose, our first approach consists in solving Maxwell's equations with proper boundary conditions in somewhat simplified domains and matching the fields over adequate coupling surfaces. We carry on an attempt of this kind in our institute for a very idealized, but still interdigital structure.

In the same time, we found it worthwhile to develop an alternate approach, based on the Marcuvitz and Schwinger analysis. It consists in defining for each mode the impedance of obstacles and apertures in the guide and their couplings by a method similar to the one described by Bethe. This technique leads to the definition of a lumped circuit with assumed values of the elements.[6] For a given model, these values can be specified later on by proper fitting to the experimental dispersion curve. This method seems particularly well suited for the IH structure, due to the moderate size of its geometrical elements as compared to the wavelength (at least in the low frequency part of the passband).

Although the results of this calculation are not directly applicable to the design of an accelerating cavity, they lead at least to a better understanding of the structure.

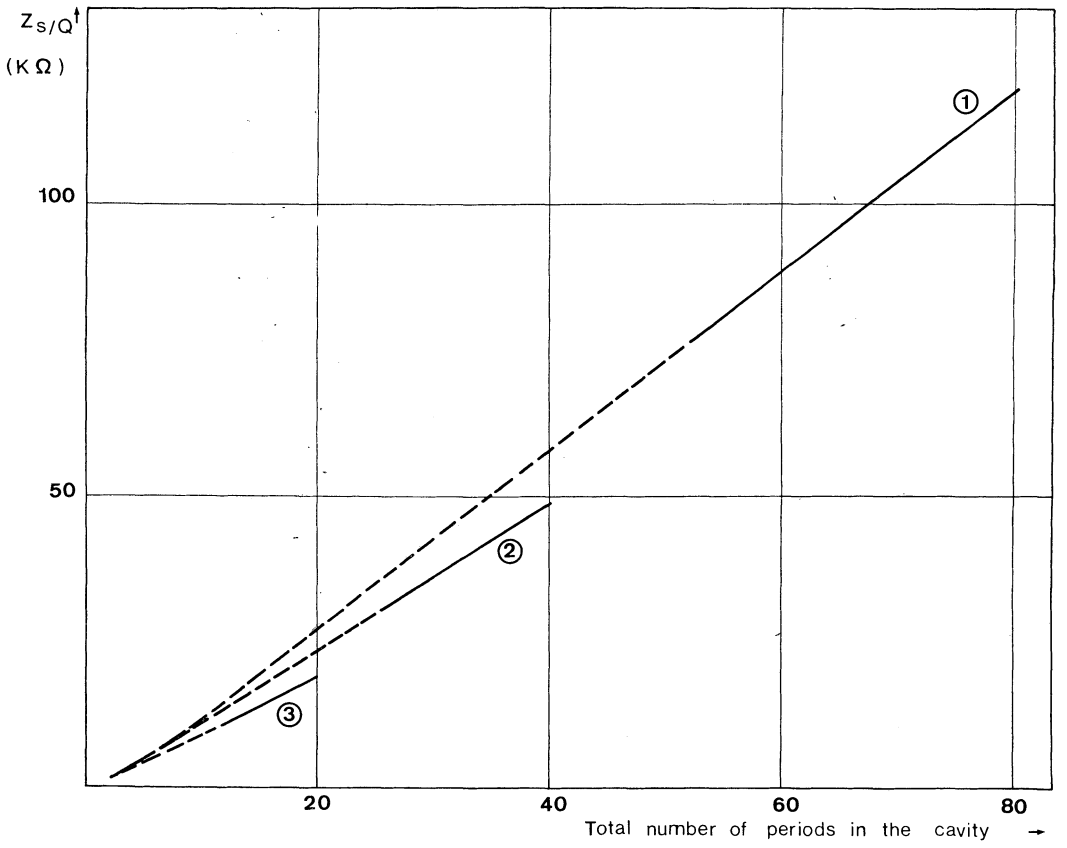

FIG. 5. Z_s/Q dependence on cavity length and energy. Drift tubes ϕ: 6.66 per cent of cavity diameter, gap to period ratio 50 per cent. For the solid part of the curves: (1) energy: 290 keV per nucleon ± 1 per cent, average Q at 27 MHz: 15 800 ± 3 per cent, (2) energy: 1.95 MeV per nucleon ± 1 per cent, average Q at 27 MHz: 15 200 ± 1.5 per cent, (3) energy: 10.15 MeV per nucleon ± 1 per cent, average Q at 27 MHz: 14 600 ± 1 per cent. The curves are deduced from experimental measurements by formula (6).

Let us now examine briefly our theoretical work by this method. Due to the inherent asymmetry of the IH structure, its properties cannot be described by a single line. Figure 6 shows the simplest possible model involving two lines (one for each row of stems) coupled through the gap impedance Z_{12}. Z_1 and Z_2 correspond to the stems of each row, which we initially assume to be different, while Z_1' and Z_2' stand for the geometrical period. This model may be easily complicated, for instance by means of inductive couplings between the successive stems of two opposite rows (Z_{12}') and also by capacitive couplings between the successive stems of a same row.

If we consider the simplest case, let $\Psi_1(n)$ and $\Psi_2(n)$ be the respective currents in the nth mesh of the first and second line. We obtain the following mesh equations:

$$\begin{cases} \frac{1}{2}[\Psi_1(n-1)+\Psi_1(n+1)-2\Psi_1(n)] \\ \quad +\left(1-\frac{1}{2}\frac{2Z_1+Z_1'+2Z_{12}}{Z_1}\right)\Psi_1(n) \\ \quad +\frac{Z_{12}}{2Z_1}[\Psi_2(n)+\Psi_2(n+1)]=0 \\ \frac{1}{2}[\Psi_2(n-1)+\Psi_2(n+1)-2\Psi_2(n)] \\ \quad +\left(1-\frac{1}{2}\frac{2Z_2+Z_2'+2Z_{12}}{Z_2}\right)\Psi_2(n) \\ \quad +\frac{Z_{12}}{2Z_2}[\Psi_1(n-1)+\Psi_1(n)]=0 \end{cases} \tag{7}$$

leading to the coupled system:

$$\left.\begin{aligned} D\Psi_1(n)+k_1^2\Psi_1(n)+D_{12}\Psi_2(n)=0 \\ D\Psi_2(n)+k_2^2\Psi_2(n)+D_{21}\Psi_1(n)=0 \end{aligned}\right\} \tag{8}$$

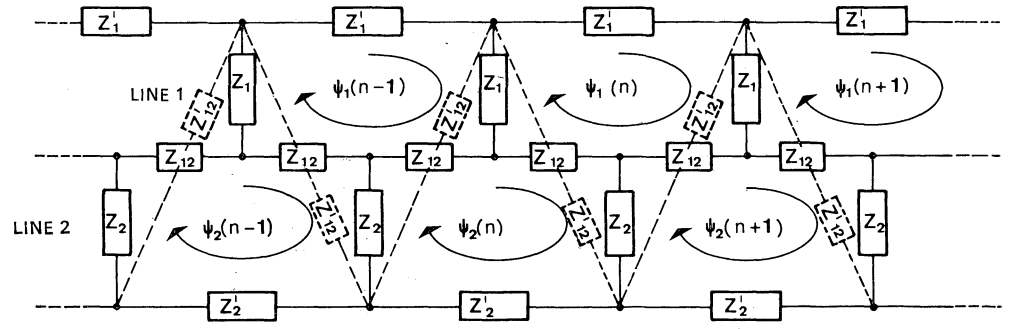

FIG. 6. Lumped elements model.

where D, D_{12} and D_{21} are operators (the last two characteristic of the interdigital nature of the structure) and the k, scalars. We must point out that k_1^2 and k_2^2 are the eigenvalues of the two lines without coupling; they are equal if the two rows of stems are identical.

If $2N$ is the total number of stems, taking into account Floquet's theorem, we can write the eigenfunctions in the form:

$$\left.\begin{aligned}\Psi_1^p(n) &= \Psi_{10}^p \exp(i(\pi/N)pn)\\ \Psi_2^q(n) &= \Psi_{20}^q \exp(i(\pi/N)qn)\end{aligned}\right\} \tag{9}$$

where p and q stand for the spatial harmonics. From system (8), and with

$$\left.\begin{aligned} f_{12} &= \frac{Z_{12}}{2Z_1},\\ f_{21} &= \frac{Z_{21}}{2Z_2},\\ \beta_q &= q\frac{\pi}{2N},\end{aligned}\right\} \tag{10}$$

where β_q represents the phase shift per accelerating period as in Section 1 (the geometrical period of each line being twice as long), we deduce the matrix equation:

$$\begin{pmatrix}\cos 2\beta_p - 1 + k_1^2 & f_{12}(1+e^{2i\beta q})\\ f_{21}(1+e^{-2i\beta p}) & \cos 2\beta_q - 1 + k_2^2\end{pmatrix}\begin{pmatrix}\Psi_1^p(n)\\ \Psi_2^q(n)\end{pmatrix} = 0 \tag{11}$$

the imaginary part of which implies $p = q$.

Then, writing:

$$F = \cos(2\beta_p) = \cos(2\beta_q) = \cos(2\beta_-), \tag{12}$$

the characteristic equation becomes quadratic and its roots may be written:

$$F_\pm = 1 + f_{12}f_{21} - \frac{k_1^2 + k_2^2}{2} \pm \tfrac{1}{2}\sqrt{(k_1^2 - k_2^2)^2 + 4f_{12}f_{21}[f_{12}f_{21} - k_1^2 - k_2^2 + 4]}. \tag{13}$$

If the two rows of stems are identical, we can write:

$$F_\pm = 1 - k^2 + f^2\left[1 \pm \sqrt{1 + \frac{2}{f^2}(2-k^2)}\right]. \tag{14}$$

Then, the case $k^2 = 2$ implies $F_- = -1$ with $dF_-/d\omega = 0$. In these conditions, $\beta = \pi/2$, and F_- is maximum or minimum, leading to a finite group velocity

$$V_g = \pm\sqrt{\frac{-F_-}{\partial^2 F/\partial\omega^2}} = \pm\frac{f}{(\partial/\partial\omega)k^2}. \tag{15}$$

When the discriminant can be zero, there is a stopband, at the boundary of which $F_+ = F_-$ with $dF_-/d\omega = -dF_+/d\omega = \infty$. If the point where $F_+ = F_-$ belongs to the interval $(-1, +1)$, the corresponding group velocity is zero (Figs. 7a and 7b). Figure 7b shows the shape of a dispersion

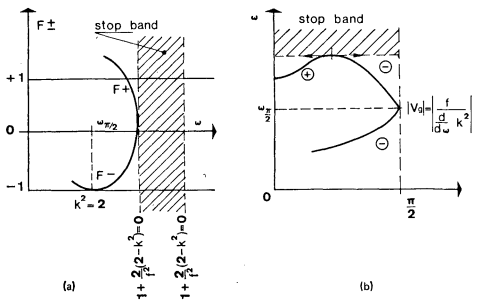

FIG. 7. Characteristic functions (a) and related dispersion curves (b) [F_+ and F_- joining inside the interval $(-1, +1)$].

curve usually found in magnetron circuits. Figures 8a and 8b show what happens when the point $F_+ = F_-$ is outside the interval $(-1, +1)$. In this case, corresponding to accelerating structures, the F_+ solution merely disappears from the dispersion curve.

When the two rows of stems are different, there are two values of $\omega(k_1^2(\omega_1) = 2$ and $k_2^2(\omega_2) = 2)$ leading to $F_- = -1$ accounting for the existence of a stopband at the $\pi/2$ mode, as shown on Figs. 8a and 8b (dotted lines). This phenomenon has been observed experimentally after perturbation of a stem row, as illustrated on Fig. 9.

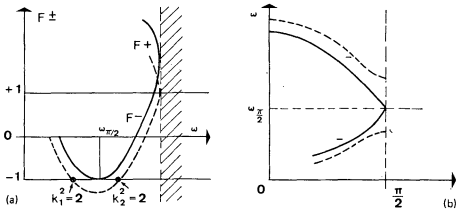

FIG. 8. Characteristic functions (a) and related dispersion curves (b) [F_+ and F_- joining outside the interval $(-1, +1)$]. Solid curves stand for the case of two identical rows of stems, and dotted curves, for two different rows, account for a stopband at the $\pi/2$ mode.

Up to now, we made no hypothesis about the nature of impedances. However, what we said about the field distribution in an IH structure suggests us to consider Z_{12} as a mere capacitance, and Z_1, Z_2, Z_1', Z_2' as mere inductances. With such a simple model, the dispersion curve passes through the point $\omega = 0$, $\beta = \pi$ (solid curve of Fig. 10). This phenomenon is not surprising since, at low frequencies, this model behaves like a bifilar line, differently from the real structure which is enclosed in the cavity walls. Then, we have to introduce the coupling (inductive) impedance Z_{12}' to re-establish a more practical situation, with a nonzero cut-off frequency at the π mode, corresponding to the dotted curve of Fig. 10. The corresponding values of the different elements can be deduced by comparison to the experimental results, also plotted on this figure.

The steepness of experimental dispersion curves near the 0 mode should result from a coupling with the Alvarez passband, coupling that could be taken into account in a more elaborate model.[7]

We also considered the case of a capacitive coupling between the successive stems of each row, which produces a significant change of the dispersion curve in the neighbourhood of the π mode.

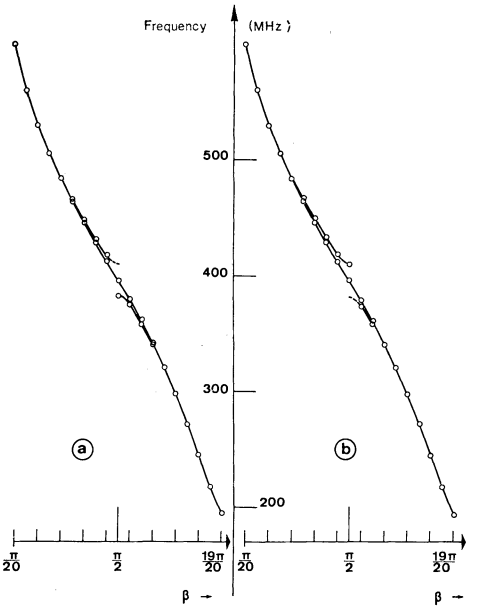

FIG. 9. Experimental proof of the existence of a stopband at the $\pi/2$ mode, when the rows of stems are different. The cavity includes 20 gaps with one row of 9 stems, the other one of 10 stems. Due to the boundary conditions, the $\pi/2$ mode corresponds to the row of 10 stems. We considered three types of stems: type 0: stems equipped with one metallic ring (close to the cavity wall), type 1: same stems without rings and type 2: same stems with two rings.

First experiment (continuous curve in a and b): both rows of type 0. Second experiment (discontinuous curve in a): 10-stems row of type 1 and 9-stems row of type-2 leading to an experimental $\pi/2$ mode at lower bound of the stopband. Third experiment (discontinuous curve in b) 10-stems row of type 2 and 9-stems row of type 1 leading to an experimental $\pi/2$ mode at upper bound of the stopband.

4. PRACTICAL CONSEQUENCES FOR HEAVY ION MACHINES

4.1 *General remarks*

Due to the constraints of multicharged ion sources, the preaccelerator voltage, the charge to mass ratio of the particles and, *a fortiori* their injection velocity remain low in a heavy ion machine. Taking into account the condition of synchronism, the choice of the frequency is then dictated by the necessity to provide housing for quadrupole lenses in the very first drift tubes.

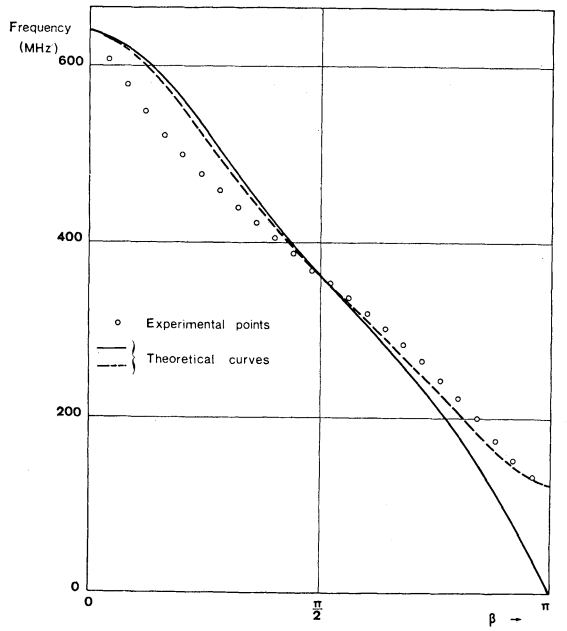

FIG. 10. Theoretical dispersion curves. In solid lines: model of Fig. 10 without Z'_{12}, for the assumed value of $Z_{12} = 1.3$ pF and $Z_1 = Z_2 = 4$ nH, $Z'_1 = Z'_2 = 144$ nH deduced from comparison with experimental results. In dotted lines: same impedances with an additional coupling $Z'_{12} = 160$ nH, showing fairly good agreement with the experimental points between $\pi/2$ and π.

The high wavelength required in order to fulfil these conditions represents one of the best arguments in favour of the IH structure which can be operated at low frequencies with reasonable transverse dimensions.

For very low energies, however, further increase of both wavelength and tank diameter seems rather unrealistic, and we plan for $3\beta\lambda/2$ operation, instead of $\beta\lambda/2$ (for instance, at 30 MHz, magnetic focusing becomes unmanageable in $\beta\lambda/2$, below about 200 keV per nucleon).

In order to illustrate the characteristics of IH structures in this range of energies, we designed such a cavity in $3\beta\lambda/2$ at 30 MHz with the following characteristics:

—input energy 56 keV per nucleon
—output energy 190 keV per nucleon
—charge to mass ratio of ions: 0.06 (normalized to protons)
—cavity length 2.71 m
mean electric field over a period: $2.6 \sin(\pi z/2.71)$ MV/m (z: abscissa of the middle of the gaps, in meters)
—number of gaps: 12
—gap to period ratio: $\frac{1}{3}$
—ϕ tank 2 m
—ϕ drift tubes 9.5 to 17.5 cm, bore diameter: 2 cm.

We shall refer to model measurements on this cavity in the next section.

The high efficiency of IH structures represents another main advantage, especially at low energy, as we shall discuss in the next section.

4.2 *Factors of merit and energy range*

The optimum energy range of IH structures can be determined taking into account shunt impedance considerations.

For this purpose, Fig. 11 summarizes the main results of our experimental investigations (Section 2.3) in terms of effective shunt impedance per unit length vs energy.

Obviously, the IH structure, tuned at 27 MHz, is fully efficient between 200 keV and 1.5 MeV per nucleon. Within these limits, it is easy, and worthwhile, to provide shunt impedance optimization, or at least to find a good compromise between shunt impedance and mechanical problems, by proper choice of the transverse geometry of the cavities.

At higher energies, as the frequency must be increased (for instance, from 27 to 54 MHz), in order to preserve reasonable tank diameters, such an optimization is no longer possible. Anyhow, an adequate choice of both frequencies and energy ranges along the successive cavities of a whole machine brings the upper limit of IH structures up to about 4.5 MeV per nucleon where the 108 MHz Alvarez undoubtedly becomes more efficient.

At low energy, the IH structure seems to be slightly more efficient than the Sloan and Lawrence structures. Anyway, since they imply different solutions to focusing problems (grid focusing for the bifilar structure, as in Orsay, or quadrupole focusing in every second drift tube, as in Unilac project[8]), we shall not develop this comparison.

For very low energies the choice of a $3\beta\lambda/2$ mode of operation leads to a considerable reduction of efficiency. Measured on a scaled model, the effective shunt impedance per unit length of the cavity described in Section 4.1 proved to be as low as 23 MΩ/m, due to the unfavourable transit time factor and to the comparatively long period.

The value of unloaded Q is very little affected by energy and remains in the neighbourhood of 15 000,

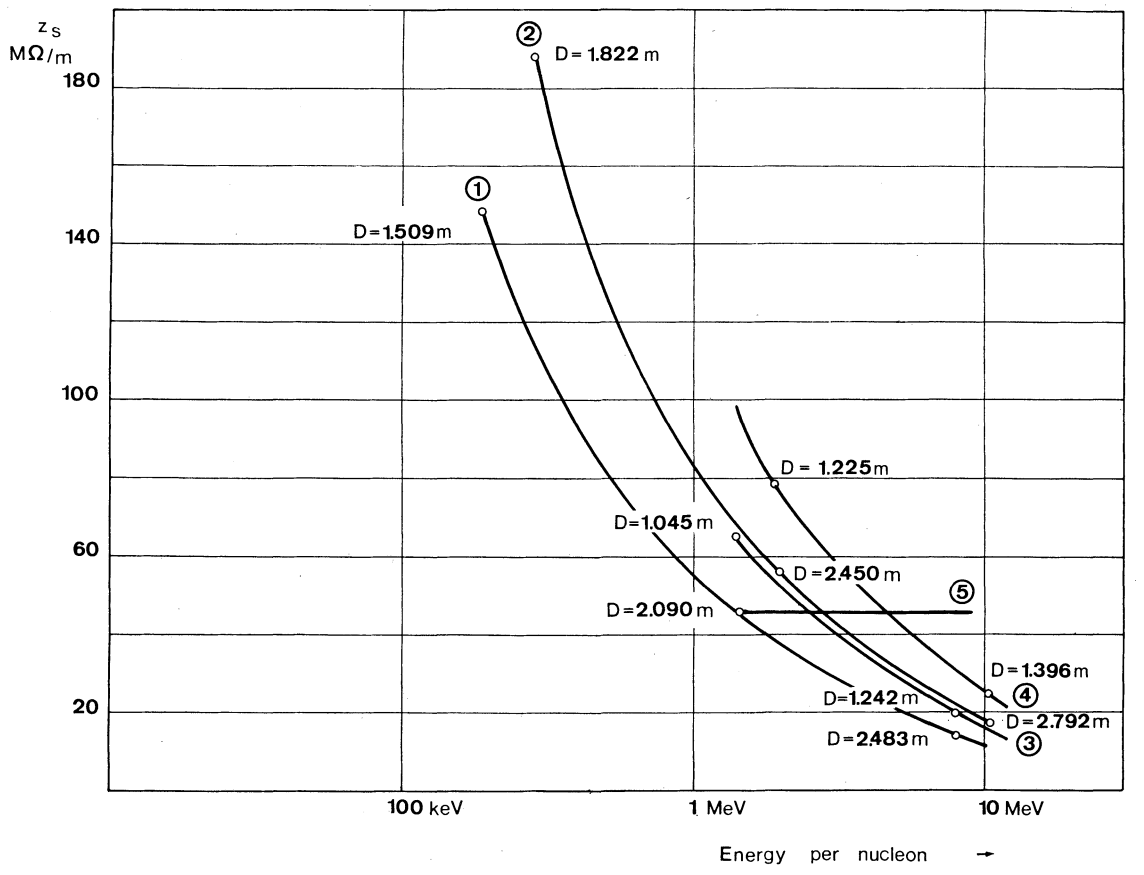

FIG. 11. Effective shunt impedance per unit length as a function of energy for $\beta\lambda/2$ operation and gap to period ratio $\frac{1}{2}$. Drift tubes ϕ: 10 per cent of cavity diameter for curves 1 and 3, 6.66 per cent for curves 2 and 4; frequency: 27 MHz, for curves 1 and 2, 54 MHz, for curves 3 and 4. For comparison, curve 5 corresponds to a 108 MHz Alvarez structure in $\beta\lambda$ (from Unilac data[7]).

at 27 MHz over the whole optimum range of the structure, even in the $3\beta\lambda/2$ case.

With respect to filling time considerations, this moderate quality factor should be regarded as an advantage of the structure, especially if the rf supply has to be pulsed.

4.3 *Focusing problems, acceptances and emittances*

From the point of view of quadrupole housing in the drift tubes, the synchronism law ($L = \beta\lambda/2$, instead of $L = \beta\lambda$) is more restrictive in an IH structure than in the Alvarez case. For the same particle velocity, drift tube length and peak accelerating field, it turns out that an Alvarez cavity (with a gap to period ratio of 25 per cent) can be operated at a frequency three times as much as the corresponding IH structure (with a gap to period ratio of 50 per cent). Even in these conditions, the Alvarez structure leads to larger transverse and longitudinal dimensions (effectively, the flat field pattern is not sufficient to compensate the low gap to period ratio) and requires stronger quadrupole gradients for focusing (between 30 and 40 per cent more than the IH structure for the same magnetic focusing system).

On the other hand, the choice of a sinusoidal field distribution still gives a good longitudinal acceptance—the shape of the curve being even more convenient than in the Alvarez case—and a quite satisfactory damping. Moreover, the slow increase of the field at low energy end of the cavity facilitates radial focusing in the shortest drift tubes. An illustration of these results, applied to the cavity described in Section 4.1 is given on Figs. 12 and 13. The radial acceptance and emittance are associated with a given, feasible, magnetic field pattern along the machine. However, in this example, we did not intend to give more than indicative results and, due

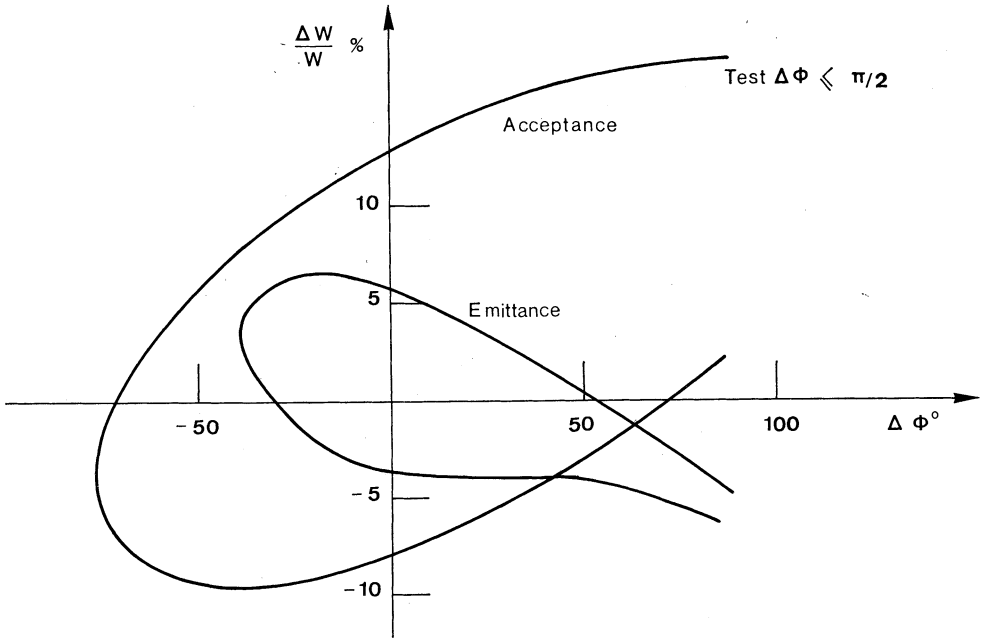

FIG. 12. Longitudinal acceptance and emittance of the cavity described in Section 4.1.

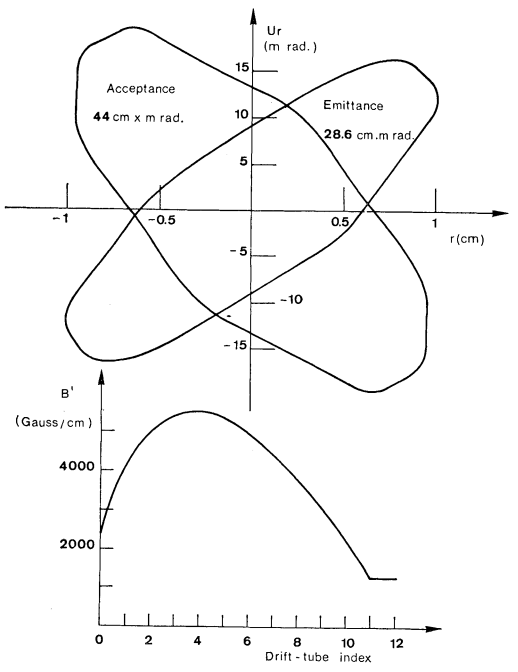

FIG. 13. Radial acceptance and emittance of the cavity described in Section 4.1 for a given + + − − focusing.

to the moderate size of our home computer, our calculations were not so accurate (for instance, no attempt has been made for radial focusing optimization) as we shall require in a final design. For the same reason, the effect of a buncher has not been taken into account on Fig. 12.

4.4. *Design of accelerating cavities and associated problems*

The results of the preceding sections show that an IH structure is suitable for particle acceleration, and especially for heavy ions below 4.5 MeV per nucleon. Let us now examine a few design problems.

Once the frequency of a cavity is chosen, its longitudinal geometry can be calculated for any given field distribution. For our part, although it is certainly possible to obtain a flat field at cut-off frequency (for instance by means of resonating terminations, instead of conventional end plates) we preferred the rather natural sinusoidal field pattern.

Then, one has to find the proper transverse dimensions of the cavity fitting the exact field law and frequency. Since we have no theoretical method available, this determination is based upon

our experimental studies on periodic structures. Practically, for any frequency and cavity length, we can convert our experimental data (after proper scaling) into a series of curves representing, for instance, the variation of cavity diameter with period length for discrete values of the other parameters.[9]

If we consider an accelerating structure as a chain of periodic sections, these curves enable us to predict the transverse dimensions of the cavity. However, this assumption being only approximate, we cannot expect very precise results from this method and, as shown on Fig. 14, further geometrical corrections, on a scaled experimental model, are still necessary for proper adjustment of the field distribution.

The determination of transverse geometry being not unique for a given cavity, it is then possible to choose the most efficient solution consistent with machining feasibility.

From the technological point of view, an IH cavity is rather similar to an Alvarez cavity. Nevertheless, we must point out two important questions related to both distribution of power losses and tolerances.

Due to the intense currents flowing along the stems, one has to take special care of rf joints (bellows between the stems and cavity walls) and also to provide efficient cooling of the stems where the main part of power losses (let us say about 70 per cent of total losses) are dissipated.

The question of tolerances is also a very important one. We represent in Fig. 15 the successive modes of an accelerating cavity (described in Section 4.1). Due to the good mode separation in the neighbourhood of the operating mode, tolerances on tuning errors should be moderate. Tolerances on drift tube position are more stringent, as shown on Fig. 14, where a poor alignment of the drift tubes is responsible for the irregularities of the field.

Till now, our experimental cavities were not

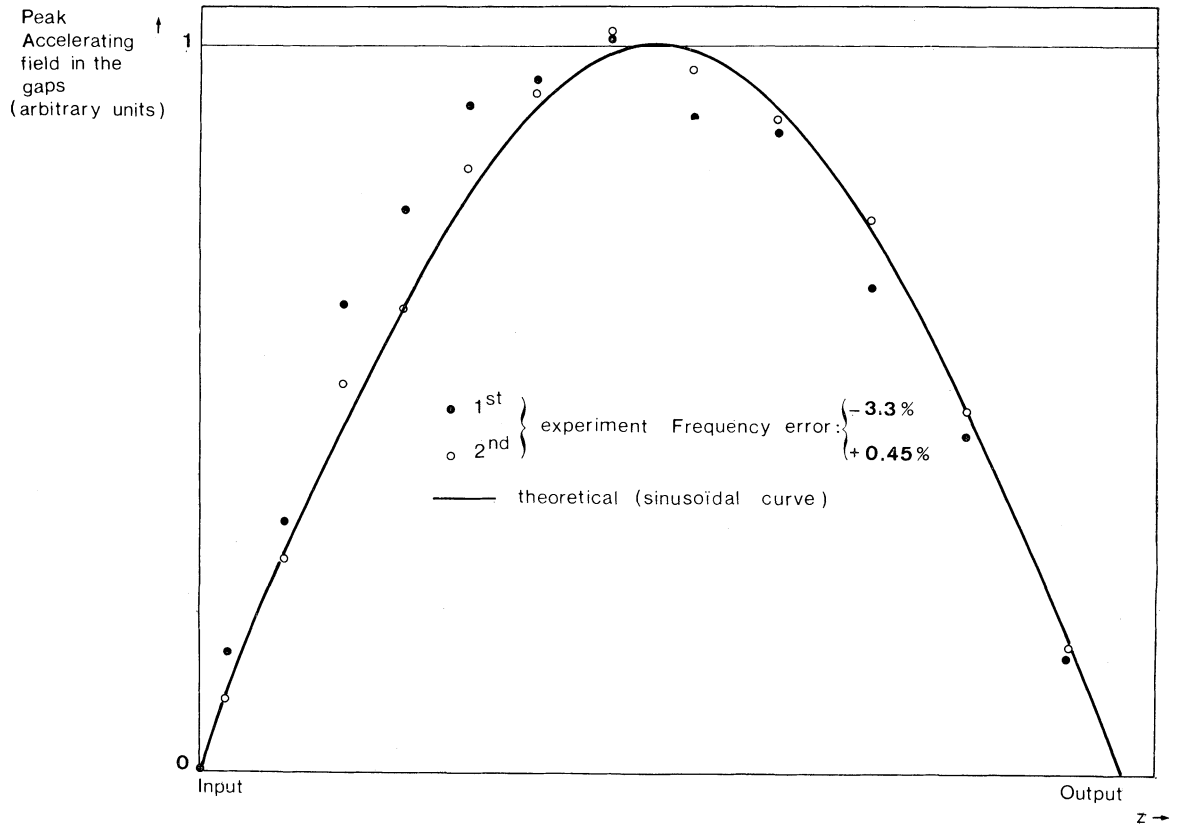

FIG. 14. Model adjustments of field and frequency for an accelerating structure. (Cavity described in Section 4.1.)

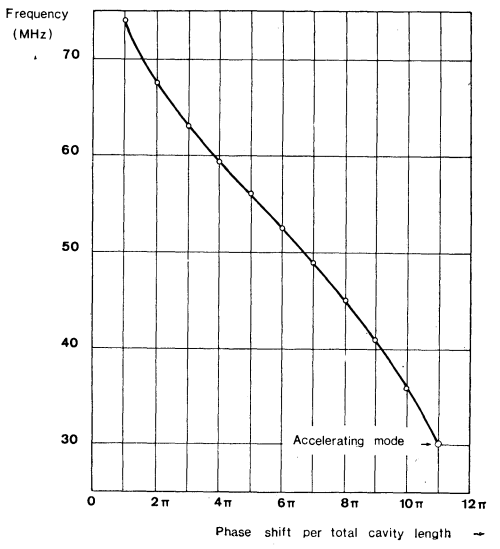

FIG. 15. Successive modes of an accelerating cavity (described in Section 4.1).

sufficiently large to allow significant investigations of this question. Our next experiment on a one-third scaled model of our first prestripper, provided with a device for proper adjustment of the drift tubes, will enable us to solve this problem in a much more precise manner.

Nevertheless, we began to study a device for fine adjustment of the field. We first planned to achieve this purpose by means of metallic rings sliding along the stems.[7] However, since the main changes of the fields distribution occur along a rather short section of the stem, the accuracy of this solution proved to be moderate. For this reason, and also to avoid a few unpleasant mechanical problems, we are now thinking of a more versatile solution, using metallic plates independent from the stems and adjustable by rotation in the magnetic field. Such devices have been provided in our next cavity model for a more precise study.

We also intend to achieve frequency regulation of the cavities in a similar way.

5. CONCLUSION

Throughout this paper, we describe the physical properties of IH structures, and discuss the feasibility and sometimes the advantages of its practical use for particle acceleration.

As shown in a recent article by Livingston,[10] the acceleration of heavy ion beams proves to be considered everywhere as a very up-to-date question. As a conclusion to this paper, we should like to say a few words about our project of a linear accelerator for heavy ions.

This machine is designed to accelerate all the ions of minimum charge to mass ratio 0.06 up to an energy of at least 7.5 MeV per nucleon.

We chose to inject then beam in the linac itself at the highest energy consistent with an open-type high voltage supply. Actually, we decided on a 1 MV injector bringing the ions up to about 52 keV per nucleon (V_{inj} = 862 kV for the heaviest ions).

The energy of stripping has been fixed at 1.5 MeV per nucleon and the prestripper is divided in two tanks. The first one, operated in $3\beta\lambda/2$ and bringing the ions up to about 190 keV per nucleon could be eventually removed, as well as the stripper itself, in the case of appearance of the highly promising new-look sources.

Since little information is still available about the stripping of very heavy ions at such energies, we designed two versions of our post-stripper: one for a solid stripper, the other one for a gas stripper. Our final choice will depend upon the experimental results from Orsay or Berkeley. In both cases, the post-stripper involves two cavities (respectively from 1.5 to 5 and from 5 to 8.5 MeV per nucleon in the solid stripper version, or from 1.5 to 4 and from 4 to 6.5 MeV per nucleon in the gas stripper version).

The variation of energy is given by the same method as in Unilac,[8] by means of 8 single-gap cavities in the first case, 10 in the second one, accounting for a continuous range from 1.5 up to 10.25 or 7.75 MeV per nucleon, respectively, for the heaviest ions.

The choice of the frequencies for the different stages of our machine (27 MHz for the prestripper, 54 MHz for the post-stripper, and 108 MHz for the variable energy part) is closely connected to the cooperation established between Heidelberg and Lyon. In these conditions, many technical problems would receive the same solution and moreover the fine structure of our beam would be the same as in Unilac, providing some advantageous standardization in the experimental surroundings of the two machines.

As a conclusion to our studies on IH structures, and also as an introduction to practical building problems, we plan to work out a full scaled model

of our first prestripper tank, which could be tested in real accelerating conditions behind a Van de Graaff machine with O_{16}^{+} that means for a charge to mass ratio of the order of 0.06.

ACKNOWLEDGEMENTS

We are deeply grateful to J.-P. Hadjout and G. Maurelli for their efficient work in the experimental part of this study. The success of our program is also due to L. Guyon, in charge of the mechanical workshop and to all the people of his department.

REFERENCES

1. J. P. Blewett, 'Linear accelerator injectors for proton synchrotrons', CERN Symposium, 1956, p. 162.
2. J. Pottier 'Une nouvelle structure à cavité résonnante pour accélérateurs linéaires d'ions', Note CEA No. 195 (1957).
3. V. A. Bomko, E. I. Revutskii, L. I. Bolotin, 'High frequency characteristics of a linear accelerator raising multicharge ions to energies of 1 MeV per nucleon in an H_{111} wave', *Soviet Physics, Technical Physics*, **9**, No. 7, 979 (1965).
4. N. E. Kovpak, L. N. Baranov, P. M. Zeidlits, 'A linear accelerator of protons with the 2.5 MeV energy on the H_{11n} wave', *Ukrainian Physics Journal*, **13**, No. 4, 552 (1968).
5. J. Pottier, 'A new structure for heavy-ions linacs', *IEEE Trans. Nucl. Sci.*, **NS-16**, No. 3, 377 (1969).
6. D. T. Tran, 'Structures accélératrices bi et tripériodiques', *Revue Technique Thomson-CSF*, **1**, No. 2, 239, juin 1969.
7. M. Bres, 'Thèse Doctorat de spécialité', Faculté des Sciences, Université de Lyon (to be published).
8. K. Blasche, D. Böhne, Ch. Schmelzer, B. Stadler, 'Unilac, a variable energy heavy ion linear accelerator', *Proc. Intern. Conf. on Nuclear Reactions Induced by Heavy Ions, Heidelberg, 1969*, p. 518.
9. A. Chabert *et al.*, 'La structure interdigitale de type H', *Comptes-rendus de la Session d'etudes sur la physique et la production des ions lourds, La Plagne, Mars 1969*, p. V.5.1.
10. R. S. Livingston, 'The acceleration of heavy ions', *Particle Accelerators*, **1**, 51 (1970).

Received 23 July 1970; and in revised form
11 September 1970